ELSEVIER

A compendium of potential energy maps of zeolites and molecular sieves

D. Keffer,* Vishwas Gupta,* David Kim,† Elizabeth Lenz,† H. Ted Davis,* and Alon V. McCormick*

**Department of Chemical Engineering and Materials Science, University of Minnesota, Minneapolis, Minnesota, United States*
†Minnesota Supercomputer Institute, Minneapolis, Minnesota, United States

We present potential maps of xenon in 20 different zeolites and molecular sieves. The potential maps reveal both the accessible pore volume and localized adsorption sites and so are important in understanding adsorption and diffusion processes in nanoporous materials. We examine zeolites and molecular sieves with one-dimensional channel-like nanopores (zeolite-Theta 1, $AlPO_4$-5, zeolite-Omega, zeolite-L, ZSM-12, $AlPO_4$-8, and VPI-5), with two-dimensional intersecting channel-like nanopores (ZSM-5 [silicalite], ZSM-11, ferrierite, mordenite, and zeolite-Beta), and with three-dimensionally connected cagelike nanopores (zeolite-A, zeolite-Rho, zeolite-Y, sodalite, chabazite, cloverite, cation-poor zeolite-A, and cation-rich zeolite-A). We report the fraction of pore volume accessible, the maximum energy well depth at the adsorption sites, and the activation energy to move between sites. We note several examples of surprising similarities and differences between various molecular sieves. In several instances, we show that these potential profiles are relevant for other small Lennard–Jones-like molecules. By comparison with published Monte Carlo and molecular dynamics simulations, we show that the density distributions of adsorbates at low density are well predicted by the potential maps.

INTRODUCTION: THE IMPORTANCE OF POTENTIAL MAPS

Potential energy maps of the nanopore space in zeolites and molecular sieves provide important information about the environment in which an adsorbate resides. These maps provide the accessible volume of the pore (which is useful in predicting Xe chemical shifts in molecular sieves.[1]) They also provide the number, location, and depth of the localized potential energy wells that constitute adsorption sites. This information is crucial in understanding and modeling adsorption and diffusion in crystalline nanoporous materials; it can also be important in understanding catalytic behavior in zeolites and molecular sieves. (As a distinction in terminology, zeolites are aluminosilicates and are a subset of molecular sieves, which also include other compositional variants, e.g., aluminophosphates or silicoaluminophosphates. In this work, when we use the term molecular sieves, we mean to include zeolites.)

Research efforts have focused on the structure of the lattice of adsorption, which is related to but distinct from the framework lattice. For instance, using Monte Carlo simulations of xenon in zeolite-A, Van Tassel et al. demonstrated the presence of a well-defined lattice of discrete adsorption sites within zeolite-A cages, which remained unchanged up to moderate adsorbate loadings.[2–5] This knowledge of the lattice of adsorption sites allowed the development of rigorous models of diffusion,[6] adsorption of single-component fluids,[7] adsorption of binary mixtures,[8] and percolative behavior.[9]

Other examples of research involving the lattice of adsorption sites include the following:

1. A lattice model for predicting the adsorption thermodynamics of benzene in silicalite has been developed by Snurr *et al.*[10], in which the adsorption lattice is based on the density distributions from Monte Carlo simulations.
2. In mordenite at various Si/Al ratios, Nivarthi et al. report lattice-like adsorption of Xe and explain that dealumination shifts the site energy but not their locations.[11]
3. We have constructed potential energy maps and density distributions of ethane and methane in the molecular sieve $AlPO_4$-5.[12] We showed that the density distributions of both ethane and methane correspond to the predictions of the potential maps. We have also demon-

Color Plates for this article are on pages 100 to 104.

Address reprint requests to: Alon V. McCormick, Department of Chemical Engineering and Materials Science, University of Minnesota, 151 Amundson Hall, 421 Washington Ave., S.E., Minneapolis, Minnesota 55455-0132.

Received 14 November 1995; accepted 4 April 1996.

655 Avenue of the Americas, New York, NY 10010

0263-7855/96/$15.00
PII S0263-7855(96)00040-9

strated that isopotential surfaces are helpful to predict roughly the onset of single-file diffusion in $AlPO_4$-5.

In this article, we demonstrate that the localized potential wells shown by potential maps correspond to the regions of high local adsorbate density in the nanopore as obtained through Monte Carlo and molecular dynamics computer simulations at low loadings. This correspondence between density distributions and potential maps is maintained up through moderate (sometimes as high as experimentally achievable) loadings. The correspondence should no doubt fail at high loadings, where adsorbate–adsorbate packing effects dominate the effect of the external potential.[13] The potential maps do, however, indicate in what situations neighboring sites are so close together that they may not be simultaneously occupied at reasonable sorbate pressures.

The generation of potential maps is a simple and inexpensive computational exercise. By comparison, the acquisition of density distributions involves much lengthier and more expensive molecular dynamics or Monte Carlo simulations. One certainly obtains more information from a simulation than from a potential map (e.g., diffusivities, pair correlation functions, and the correct suppression of adsorption at high loading due to crowding) but potential maps can suffice to gain insight into the location, number, and depth of the adsorption sites. In this article we provide the potential maps of xenon in 20 nanoporous materials. From these maps we determine the fraction of pore volume accessible, the maximum potential well depth, and the activation energy to move from site to site at low loading. We show in several instances that the results for xenon can be generalized to other small Lennard–Jones-like adsorbates.

The adsorbents we examine here represent a broad cross-section of nanoporous materials, including those with one-, two-, and three-dimensional porous networks. By one-dimensional nanopores, we mean molecular sieves with a network of generally cylindrical (channel-like) pores running parallel to each other in only one direction of the molecular sieve (e.g., $AlPO_4$-5). By two-dimensional channels, we mean molecular sieves with generally cylindrical pores running in two directions of the molecular sieves (e.g., silicalite), although not necessarily continuous (e.g., mordenite). By three-dimensional cages, we mean molecular sieves with an array of distinct nanopores connected to other cages via windows or short channels, forming a 3-D network (e.g., zeolite-A). We exclude molecular sieves with cations whose presence substantially alters the accessible pore volume. The principal reason for this is that it is not clear in most instances what partial charge to assign to such cations. The one exception to this is zeolite NaA, for which we have previously shown reasonable polarization energy values. For each category of nanopores, we sample a range of pore sizes, ranging from channels formed by 8 tetrahedral (T) atoms (Si, Al, or P atoms) to windows formed by 20 T atoms.

METHOD: THE ORIGIN OF POTENTIAL MAPS

Framework atom positions of the molecular sieves are obtained from the literature.[14–30] The nominal channel and cage sizes cited are taken from Ref. 31 and represent "free" distances from the van der Waals surface of an oxygen atom at one side of the pore to the van der Waals surface of an oxygen atom at the other side. We calculate the potential energy due to the presence of all the framework atom positions on an adsorbed Xe residing at each point on a three-dimensional grid inside the nanopore. The adsorbate-pore potential, $U_{ap}(\mathbf{r})$, at any grid point is given by the pairwise additive Lennard–Jones 12–6 potential.

$$U_{ap} = \sum_{i=1}^{N_f} U_{ij} = \sum_{j=1}^{N_f} 4\epsilon_{ij}\left[\left(\frac{\sigma_{ij}}{r_{ij}}\right)^{12} - \left(\frac{\sigma_{ij}}{r_{ij}}\right)^{6}\right] \quad (1)$$

where N_f is the number of framework oxygen atoms included in the calculation, ϵ_{ij} and σ_{ij} are the Lennard-Jones energy and size parameters, and r_{ij} is the distance between the adsorbate xenon (atom i) and the framework oxygen (atom j). In this way, we map the potential energy surface inside the nanopore, $U_{ap}(\mathbf{r})$. Parameter values are calculated from the Kirkwood–Muller formula using polarizabilities (Xe = 4.01×10^{-24} cm^3, O = 0.85×10^{-24} cm^3) and van der Waals radii (Xe = 2.05 Å and O = 1.52 Å).[3]

Consistent with previously justified practices, we consider only the interaction due to the oxygen, neglecting Si, Al, and P contributions to the external potential.[32] We also neglect any partial charges on the oxygen, as the resulting polarization energies have been shown to be small in magnitude compared to the dispersive and repulsive terms in the potential.[33] We primarily consider cation-free adsorbents. If the adsorbent typically has cations, we model the purely siliceous analog.

The lattices are modeled as rigid. In simulations with dynamics lattices, Demontis et al. have shown that adsorbate-oxygen radial distribution function is nearly the same in both rigid and flexible lattices, thus implying that the adsorbate placement is not strongly affected by the thermal motion of the oxygen.[34]

The potential maps are visualized using Explorer software on a Silicon Graphics workstation.

RESULTS: THE MEANING OF POTENTIAL MAPS

For three molecular sieves, chosen to represent one-, two-, and three-dimensional porespaces ($AlPO_4$-5, silicalite, and zeolite-Y), we show two three-dimensional potential map contour plots: (1) a plot with a high-energy surface (U_{ap} = 0) enclosing all of the pore space where the adsorbate has a negative energy of adsorption with respect to an ideal gas, and (2) one with a low-energy surface ($U_{ap} < 0$) that indicates the number and position of the potential energy wells. In these illustrations (see Color Plates 1–20), the surfaces represent contours of constant energy. Inside the surfaces are volumes with lower (more favorable) energy. For the remaining 17 molecular sieves, we show only the low-energy surface, which shows the potential wells. Figures showing the accessible volumes in the remaining molecular sieves are available for viewing at http://www.cems.umn.edu/~zeolites.

For the low-energy (site) plots, the value of U_{ap} chosen for the isopotential surface varies from adsorbent to adsorbent, reflecting the different site energies. In some cases the sites are distinct points, whereas in other cases the sites are

continuous rings or strings. We chose a value of U_{ap} that best reflects the geometry of the deepest wells (with energy barriers less than 2 kJ/mol within the sites).

We present the fraction of accessible volume, the maximum well depth, and the site-to-site activation energy (the difference between the well depth of a site and the maximum energy encountered moving along a minimum energy path to an adjacent site) for each molecular sieve in Table 1.

A. One-dimensional channel-like nanopores

1. Zeolite-theta 1 Theta 1 has one-dimensional 10-ring channels (composed of 10 T atoms and 10 O atoms) of nominal major and minor axes of 4.4 and 5.5 Å. The accessible volume, contained within the $U_{ap} = 0$ surface, is a tube that weaves down the center of the channel. The tube has a variable diameter along the pore axis and is not centered in the pore. In Color Plate 1, we show the two adsorption sites, contained in the $U_{ap} = -43.2$ kJ/mol surface, per unit cell length of a channel. The lowest energy path between sites is approximately a straight line.

2. ZSM-12 ZSM-12 has one-dimensional 12-ring channels of oblong cross-section with nominal axes of 5.5 and 6.2 Å. The accessible volume reflects the oblong cross-section of the channel. In Color Plate 2 ($U_{ap} = -28.3$ kJ/mol), the adsorption sites are discrete points, as in Theta-1. The energy wells in ZSM-12 are less deep than in the 10-ring channel of Theta 1. The minimum energy path from site to site is not a straight line but instead roughly follows the surface of the accessible volume tube.

3. Zeolite-omega Like ZSM-12, zeolite-Omega (isomorph of mazzite) has one-dimensional 12-ring channels. However, the channels of Omega are more circular in cross-section with a nominal diameter of 7.4 Å. The accessible volume is a tube centered in the pore with varying diameter, it is widest to either side of the 12-ring and narrowest at the 12-ring. The adsorption sites (Color Plate 3 [$U_{ap} = -26.8$ kJ/mol]) are toroids located on either side of the 12-rings. The maximum well depth is similar to that in ZSM-12. The lowest energy path between sites again follows the surface of the accessible volume tube.

4. $AlPO_4$-5 Like zeolite-Omega, $AlPO_4$-5 has one-dimensional 12-ring channels with nominal diameter of 7.3 Å. The features of the accessible volume in Figure 1 ($U_{ap} = 0.0$ kJ/mol) and the adsorption sits in Color Plate 4 ($U_{ap} = -21.5$ kJ/mol) are analogous to those of Omega. As expected, since the unit cell length of $AlPO_4$-5 (8.5 Å) is slightly larger than that of Omega (7.6 Å), the toroidal-shaped adsorption sits are farther apart. The diameters of the potential well rings are nearly the same as in Omega but the wells are deeper and the activation energy to move from ring to ring is greater in Omega.

Table 1. Accessible volumes and maximum well depths

Adsorbent	Accessible volume $\left(\frac{\text{accessible volume}}{\text{adsorbent volume}}\right)$	Maximum well depth (kJ/mol)	Activation energy (kJ/mol)
1. Zeolite-theta 1	0.0437	45.6	3.1
2. ZSM-12	0.0389	32.9	7.2
3. Zeolite-omega	0.0541	33.3	10.5
4. $AlPO_4$-5	0.0997	26.8	6.4
5. Zeolite-L	0.117	33.4	19.1
6. $AlPO_4$-8	0.383	25.9	3.9
7. VPI-5	0.328	29.4	11.0
8. Ferrierite	0.0941	34..4	6.4
9. Silicalite	0.104	33.1	6.4/10.1[a]
10. ZSM-11	0.102	34.4	8.6/11.2[b]
11. Mordenite	0.109	26.6/39.5[c]	4.6/14.7[d]
12. Zeolite-beta	0.183	28.5	8.6
13. Chabazite	0.133	36.4	16.3
14. Cation-free A	0.206[e]	24.4	4.2[f]
15. Zeolite-rho	0.159	39.5	21.1
16. Zeolite-Y	0.175	18.2/16.2[g]	4.4
17. Cloverite	0.298	43.9	—
18. Cation-poor mordenite	0.0986	37.0/89.0[c]	6.0/52.0[d]
19. Cation-poor A	0.174	55.1	11.0
20. Cation-rich A	0.142	55.1	13.8

[a]The two activation energies for silicalite are for moving along the straight channel and sinusoidal channel, respectively.
[b]The two activation energies for ZSM-11 are for moving along a straight channel and for changing channels at an intersection.
[c]The two well depths in mordenite are for main-channel and side-pocket sites, respectively.
[d]The two activation energies in mordenite are for moving along the main channel and for leaving the side pockets, respectively.
[e]The accessible volumes for cation-free, cation-poor, and cation-rich A and Y include the sodalite cages.
[f]For all of the three-dimensional cagelike zeolites, the activation energies are for intracage motion.
[g]The two well depths in zeolite- Y are for the 4R and 6R sites, respectively.

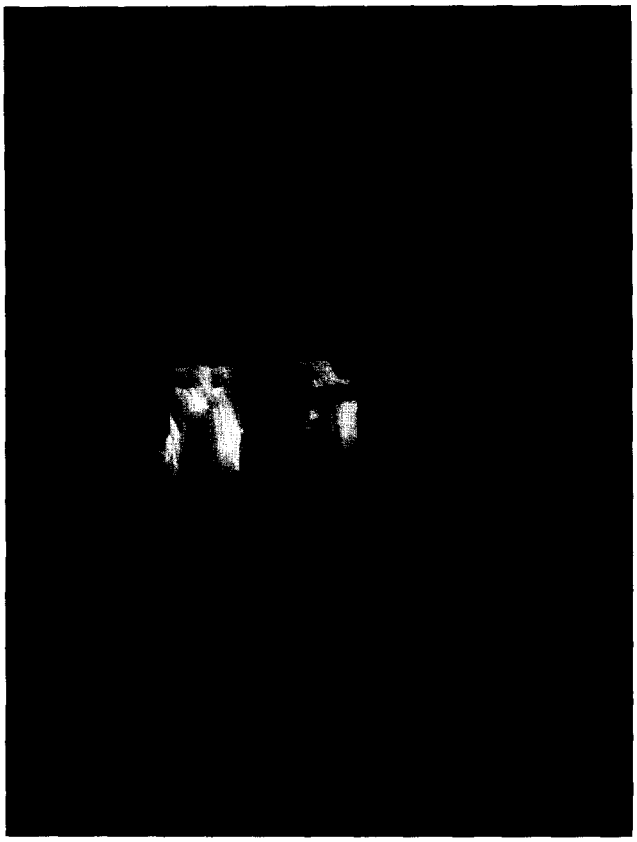

Figure 1. $AlPO_4$-5: Isopotential surface of xenon. $U_{ap} = 0$.

The adsorption sites for xenon are analogous to those reported for methane and ethane in $AlPO_4$-5,[12] indicating that the potential maps for xenon are meaningful for other small Lennard–Jones-like molecules.

5. Zeolite-L Like $AlPO_4$-5 and Omega, zeolite-L has one-dimensional 12-ring channels with an only slightly smaller nominal diameter of 7.1 Å. However, L has only one 12-ring per unit cell length of channel. The diameter of the accessible volume tube varies more widely than in either $AlPO_4$-5 or zeolite-Omega, and so the toroid adsorption sites are larger in diameter in L (Color Plate 5 [U_{ap} = −23.0 kJ/mol]). Since there is only one 12-ring per unit channel, there is only one toroid adsorption site per unit cell length of channel. (In Color Plate 5, the two halves of the site are shown.) The toroid adsorption sites of L are about as deep as those in Omega but they are separated by a higher energy barrier than those in either $AlPO_4$-5 or zeolite-Omega. The minimum energy path from ring to ring is again along the surface of the accessible volume tube.

6. $AlPO_4$-8 The nanopores in $AlPO_4$-8 are oblong one-dimensional 14-ring channels, with nominal axes of 7.9 and 8.2 Å. These channels are larger than the previous four 12-ring sieves. The accessible volume is rectangular in shape. The adsorption sites are two parallel strings that weave down the channel, connecting periodically (Color Plate 6 [U_{ap} = −20.2]). The wells are not as deep as those in the 10- or 12-ring channels. As indicated by the continuous site, the activation energy to move down the pore is small.

7. VPI-5 The nanopores in VPI-5 (isomorph of $AlPO_4$-54) are one-dimensional 18-ring channels, with a nominal diameter of 12.1 Å. The accessible volume and adsorption sites are similar in shape but are larger than those in the 12-ring $AlPO_4$-5. The adsorption sites are toroids situated between the 18-rings, as shown in Color Plate 7 (U_{ap} = −18.7 kJ/mol). The minimum energy path moves along the surface of the accessible volume.

General trends of one-dimensional molecular sieves Several general trends are exhibited by these one-dimensional molecular sieves: (1) Pores are not cylindrical but rather are undulating tubes. The minimum nominal diameter, given by the placement of oxygen in the ring, is not an accurate measure of either accessible volume or site volume. For channels with circular cross-sections, the adsorption sites are typically toroids; (2) as one might expect, however, the fraction of accessible volume increases with increasing number of T atoms in the ring that defines the channel, e.g., VPI-5 (with 18-rings) has more accessible volume than zeolite-Theta (with 10-rings). For pores of the same size, ($AlPO_4$-5, L, Omega, and ZSM-12—all 12 rings), the differences in accessible volume depend on the particular structure of the molecular sieve; (3) in general, smaller pores (less accessible volume) have deeper potential wells. For pores of the same nominal diameter, the differences in well depth again depend on the detailed structure of the molecular sieve; and (4) the deeper wells of smaller pores generally cause a higher activation energy for motion along the channel. It is noteworthy, however, that the activation energy does not necessarily increase with increasing distance between sites.

B. Two-dimensional intersecting channel-like nanopores

8. Ferrierite The network of nanopores in Ferrierite is composed of a two-dimensional array of channels. Along the [001] axis, there are 10-ring straight channels of ellipsoidal cross-section with nominal principal axes of 4.2 and 5.4 Å. Along the [010] axis, there are 8-ring ellipsoidal straight channels with nominal principal axes of 3.5 and 4.8 Å. The accessible volume tube is nearly cylindrical along the 10-ring channels but is barely continuous along the 8-ring channels (i.e., xenon barely fits). In Color Plate 8 (U_{ap} = −30.0 kJ/mol), the adsorption sites are deepest and are hexagonal rings in the 8-ring channels but there are also smaller discrete sites in the 10-ring channel. There are no sites in the intersections.

9. Silicalite The network of nanopores in silicalite (siliceous analog of ZSM-5) is composed of a two-dimensional array of channels. Along the [010] axis, there are 10-ring straight channels with nominal diameter of 5.3 to 5.6 Å. Along the [100] axis, there are 10-ring sinusoidal channels with nominal diameter of 5.1 to 5.5 Å. Figure 2 (U_{ap} = 0) shows that the accessible volume is nearly cylindrical along the straight channels. In Color Plate 9 (U_{ap} = −29.8 kJ/mol), deep adsorption sites exist in both sets of channels. Shallower sites are in the intersections. The potential wells in silicalite are approximately of the same depth as those in ferrierite.

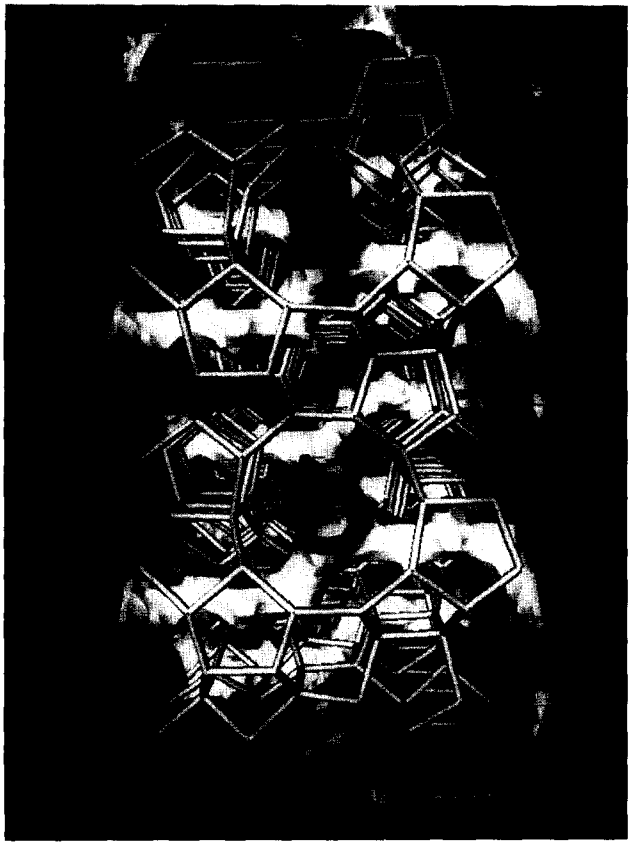

Figure 2. Silicalite: Isopotential surface of xenon. $U_{ap} = 0$.

Mapping of the potential of silicalite has been done for xenon, methane, propane, butane, hexane, water, methanol, benzene, toluene, *p*-xylene, and SF_6.[35–44] These works all agree in predicting the same number and position of sites in the straight and sinusoidal channels as well as in the intersections (although the relative favorability of the three types of sites varies with adsorbate). This observation again suggests the transferability of potential maps for Xe to other small adsorbates. Simulations of longer alkanes in silicate, however, show that once the molecules reach a certain length the density distribution no longer correlates with the potential map.[45,46]

10. ZSM-11 Like silicalite, ZSM-11 has a two-dimensional array of channels, both of which are 10-rings with nominal diameters of 5.3 to 5.4 Å. The difference between the two zeolites is that in ZSM-11 all channels are straight. Color Plate 10 (U_{ap} = −32.2 kJ/mol) shows that the adsorption sites are similar in both sets of channels. As in silicalite, there are sites in the channels and at the intersections. The well depth in ZSM-11 is approximately the same as that in silicalite.

11. Mordenite Before dealumination, mordenite is typically considered a one-dimensional zeolite composed of main channels with side pockets (which are blocked by cations and so do not constitute channels). We examine the cation-free (dealuminated) analog of mordenite, however, and we include it as a two-dimensional zeolite. Even though the secondary channels are not continuous, they provide the channel intersections, which are characteristic of two-dimensional molecular sieves.

The principal axes of the ellipsoidal 12-ring main channel are 6.5 and 7.0 Å. The accessible volume includes a cylinder down the main access with entrances into the side-pockets. As shown in Color Plate 11 (U_{ap} = −23.9 kJ/mol), there are eight adsorption sites per unit cell length of mordenite: one in each of the two side pockets, one in the main channel in front of each side pocket, and four more in the channels. The six sites in the channel form an octahedron. The side-pocket is the most favorable adsorption site.

The adsorption sites are at exactly the same position (although of different energy) as those found by Nivarthi et al. using Monte Carlo simulations, including cations.[11]

12. Zeolite-beta Zeolite-Beta (polymorph A)[26] has a two-dimensional network of 12-ring straight channels with nominal principal axes of 7.6 and 6.4 Å along [010] and [100]. The accessible volume are intersecting cylinders running in two direction, reflecting the pore structure. The energy wells are strips located in both sets of channels, as shown in Color Plate 12 (U_{ap} = −22.0 kJ/mol). There is no energy well at the channel intersections, since the larger size of the channels and the commensurate larger size of the intersections weaken the adsorbate–framework interaction.[13] The well depth in Beta is less deep than that in the smaller 10-ring two-dimensional molecular sieves discussed above.

General trends of two-dimensional molecular sieves The trends exhibited by the two-dimensional molecular sieves are similar to those for one-dimensional molecular sieves: (1) The depth of the energy wells is generally deeper in the channels than in the intersections. The intersections, however, break up the symmetry of the toroidal sites we would see in analogous one-dimensional channels; (2) the accessible volumes are tubes of oscillating size. The nominal channel sizes do not adequately characterize the accessible volume or site volume; (3) as the channel diameter increases, the accessible volume increases; (4) as the channel size increases, the well depth becomes less favorable; and (5) the activation energies are generally larger in smaller channels.

C. Three-dimensional cage-like nanopores

13. Chabazite The network of nanopores in chabazite is composed of a three-dimensional array of cages hexagonally connected by 8-ring windows (nominal diameter of 3.8 Å) to six other cages. The accessible volume shows the cages are connected by thin links. Each cage has two irregularly shaped adsorption sites (Color Plate 13 [U_{ap} = −23.9 kJ/mol]).

14. Cation-free zeolite-A The network of nanopores in cation-free zeolite-A is composed of a three-dimensional array of approximately spherical α-cages (nominal diameter of 12.3 Å) cubically connected by 8-ring windows (nominal diameter of 4.1 Å). The cages of zeolite-A are larger than those of chabazite. The accessible volume is approximately spherical with extensions through the windows. (The volume depicted in the corners of Color Plate 14 resides in the sodalite cages, which is experimentally inaccessible.) In one

α-cage there are 14 adsorption sites (Color Plate 14 [U_{ap} = −20.8 kJ/mol]). The deepest six are centered in front of the 8-ring windows. The other eight are located in front of the six-member rings. Together they form a distorted face-centered-cubic adsorption lattice. The wells in cation-free zeolite-A are not as deep as those in the smaller chabazite.

15. Zeolite-rho Like zeolite-A, Rho is composed of cubically connected α-cages (nominal diameter of 12.3 Å) but they are connected by short 8-ring channels (one Si–O–Si bond long and 3.6 Å in diameter). The accessible volume is approximately cubic with extensions through the windows. There are 20 adsorption sites, including the 14 described for cation-free zeolite-A plus 6 more in the channels connecting cages (Color Plate 15 [U_{ap} = −20.6 kJ/mol]). The depth of the sites in the cage is approximately the same as in cation-free zeolite-A but the channel sites in Rho are deeper.

The sits here are nearly identical to those found by observing the trajectories of krypton, argon, and xenon from molecular dynamics simulations in zeolite-Rho.[47,48]

16. Zeolite-Y Zeolite-Y (isomorphic with faujasite) has roughly spherical nanopores (nominal diameter of 12.4 Å) tetrahedrally connected by 12-ring windows (nominal diameter of 7.4 Å) The cages of Y are about the same size as those of A and Rho but the windows connecting them are much larger and there are only four, instead of six windows. The accessible volume is approximately spherical with much larger extensions through the windows than found in zeolite-A or zeolite-Rho because in zeolite-Y the window is a 12-member ring instead of an 8-ring (Figure 3 [U_{ap} = 0]). There are 10 adsorption sites in a cage of zeolite-Y (Color Plate 16 [U_{ap} = −16.0 kJ/mol]). The deepest six are located in front of the center 4-ring between windows. The other four are located in front of the 6-rings.

Simulations of xenon, methane, benzene, and a variety of other aromatics have been conducted in zeolite-Y or its isomorphs, zeolite-X and faujasite.[49–61] The 4-ring sites have been shown previously for methane[51] and xenon.[53] Both 4-ring and 6-ring sites as well as the relative favorability of the sites has been shown with Monte Carlo simulations of xenon.[61] The 6-ring sites and a window site have been found for benzene.[54] When cations are included, the sites lie in front of the cations i.e., in the 6-ring sites.[50] There is evidence that the energetic barrier to intercage diffusion in Y, a feature of the potential map, depends on the radial position of the adsorbate.[58,59] In this respect, xenon primarily resides near the wall and would experience a positive intercage activation energy. It is interesting to note that for *m*-nitroaniline in zeolite-Y, X-ray powder diffraction shows the nitro group in a 6-ring site and the amino group in a 4-ring site,[60] suggesting that the potential maps for xenon may be useful for more complicated molecules.

17. Cloverite Cloverite has both a network of α and *rpa* cages and a distinct network of larger cages with 20-member windows. The accessible volume extends through the network of α-cages as well as through the separate network of larger cages. The deepest sites are in the α-cages and along the wall of the larger central cage (Color Plate 17 [U_{ap} = −18.0 kJ/mol]). The pore volume in the center of the large cage is not as favorable as that near the wall or in the α-cages because it does not have the attractive interaction of O atoms lying within a few angstroms on all sides as the smaller pores do.

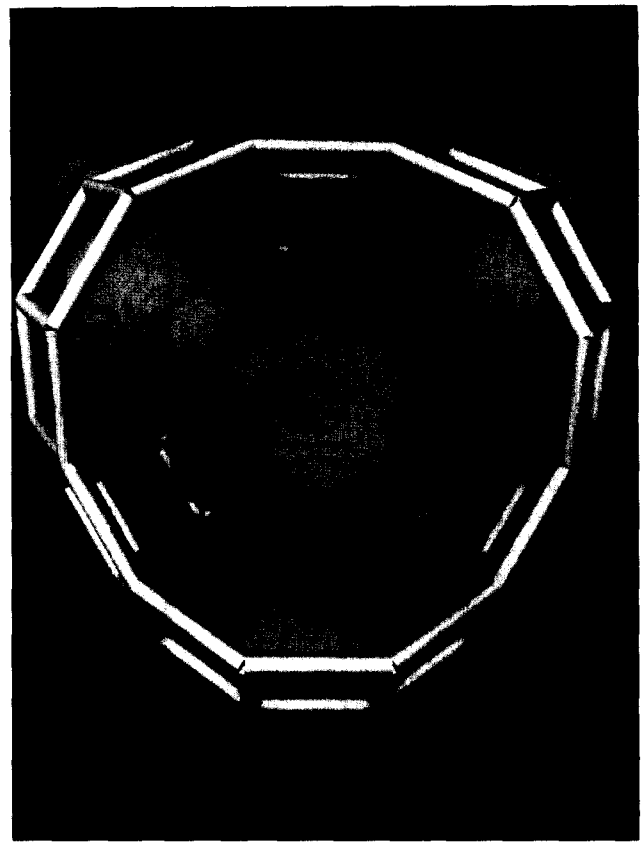

Figure 3. Zeolite-Y: Isopotential surface of xenon. $U_{ap} = 0$.

General trends of three-dimensional molecular sieves

In several ways, the trends exhibited by the three-dimensional molecular sieves are similar to those for one- and two-dimensional molecular sieves: (1) As the cage diameter increases, the accessible volume increases; and (2) as the cage size increases, the well depth becomes somewhat less favorable. In large pores like those of cloverite, however, the placement of adsorption sites is no longer sensitive to the shape of the cage. Instead, the sites are simply located next to the pore wall.

There are also distinct differences between three-dimensional and one- and two-dimensional molecular sieves: (1) The accessible volumes are spherelike shapes linked through the windows by tubes whose width reflects the size of the window; and (2) the inter-cage activation energies depend on the size of the windows linking cages.

D. Cation-containing nanopores

To conclude our survey of molecular sieves, we include cation-poor mordenite with a Si/Al ratio equal to 11, cation-poor zeolite-A, and cation-rich zeolite-A. We choose to include cations in these molecular sieves because we can compare with simulations.[2–5,11] We use the same partial charges on the sodium cations and the oxygen as was employed in the published simulations.

18. Cation-poor mordenite Cation-poor mordenite with

a Si/Al ratio equal to 11 has four cations per unit cell. The accessible volume of the cation-poor and cation-free mordenite (Si/Al = ∞) are nearly identical. The number and arrangement of adsorption sites in cation-poor mordenite (Color Plate 18 [U_{ap} = −35.0 kJ/mol]) are also the same as in cation-free mordenite, again in agreement with simulations.[11] This suggests that the potential maps here are applicable to cation-containing species so long as the cations reside in a volume inaccessible to the adsorbate. The depth of the wells is substantially deeper and, in fact, unrealistically deep. This shortcoming is due to the unavailability of a suitable model potential for cations in molecular sieves. Nevertheless, the shortcoming manifests itself only in the depth of the sits and not in their number or arrangement.

19. Cation-poor zeolite-A Cation-poor zeolite-A has eight cations placed in 6-rings at the corners of each α-cage. The accessible volume is similar to that of cation-free zeolite-A, except that there are small indentations in it owing to the cations. There are six adsorption sites placed in front of the windows, corresponding to the deepest sites in cation-free A (Color Plate 19 [U_{ap} = −49.6 kJ/mol]). This arrangement of sites exactly matches the density distribution obtained from Monte Carlo simulations in cation-poor zeolite-A.[5]

20. Cation-rich zeolite-A In addition to the eight cations per α-cage of the cation-poor analog, cation-rich zeolite-A has cations located in each 8-ring window. The accessible volume is further reduced from that of cation-poor zeolite-A by the additional cations. There are 12 adsorption sites located in front of the 4-member rings (Color Plate 20 [U_{ap} = −43.2 kJ/mol]). This arrangement of sites exactly matches the density distribution obtained from Monte Carlo simulations in cation-rich zeolite-A.[5]

The effect of including cations on the potential map depends on the location of the cations in the framework. If the cation resides in a position inaccessible to the adsorbate, the effect of the cation is to deepen the wells closest to it, without changing the number or arrangement of sites, e.g., the mordenite Si/Al ratio equals 11. However, if the cation resides in a position otherwise accessible to the adsorbate, then the number and location of sites may change in addition to the well depth, e.g., cation-rich zeolite-A.

CONCLUSIONS: USE OF POTENTIAL MAPS

The purpose of presenting this compendium of potential maps of zeolites and molecular sieves is to allow the visualization of the placement of simple adsorbates in the nanopores. The location, number, depth, and shape of the adsorption sites are shown in the potential maps. From these maps, we have calculated accessible volumes, energies of adsorption, and site-to-site activation energies.

Where comparisons with Monte Carlo or molecular dynamics simulation are available ($AlPO_4$-5, mordenite, silicalite, zeolite-A, zeolite-Rho, and zeolite-Y), the number and arrangement of potential energy wells (based on these maps at infinite dilution) agree well with the number and arrangement of adsorption sites (based on density distributions).

These potential maps are instrumental in creating accurate models of diffusion and adsorption of single-component fluids as well as mixtures. They can also be used to give a general idea of what molecular sieve might best suit any particular process, preliminarily narrowing down the number of adsorbates to be tested and pursuing those that seem most suitable.

Availability: Color images of the potential maps presented here (as well as many more views, contour levels, density distributions, and accessible volumes) are available in Ref. 62 and at the World Wide Web Compendium of Zeolite and Molecular Sieve Maps located at http://www.cems.umn.edu/~zeolites.

ACKNOWLEDGMENTS

We acknowledge the Minnesota Supercomputer Institute and NSF (CTS-9058387). David Kim and Elizabeth Lenz were supported by the Minnesota Supercomputer Institute Undergraduate Intern program. We also thank Dr. Sriram Nivarthi for his enlightening discussions.

REFERENCES

1 Gupta, V., Kim, D., Davis, H.T., McCormick, A.V. ^{129}Xe NMR chemical shifts in zeolites: Effect of loading studied by Monte Carlo simulations. In preparation (1996)

2 Van Tassel, P.R., Davis, H.T., and McCormick, A.V. Open-system Monte Carlo simulations of Xe in NaA. *J. Chem. Phys.* 1993, **98,** 8919–8928

3 Van Tassel, P.R., Davis, H.T., and McCormick, A.V. Monte Carlo calculations of adsorbate placement thermodynamics in a micropore: Xe in NaA. *Mol. Phys.* 1991, **73,** 1107–1125

4 Van Tassel, P.R., Davis, H.T., and McCormick, A.V. Monte Carlo calculations of Xe arrangement and energetics in the NaA alpha cage. *Mol. Phys. 1992,* **76,** 411–432

5 Van Tassel, P.R., Phillips, J.C., Davis, H.T., and McCormick, A.V. Zeolite adsorption site location and shape shown by simulated isodensity surfaces. *J. Mol. Graphics* 1993, **11,** 180–184, 188

6 Van Tassel, P.R., Somers, S.A., Davis, H.T., and McCormick, A.V. Lattice model and simulation of dynamics of adsorbate motion in zeolites. *Chem. Eng. Sci.* 1994, **49,** 2979–2989

7 Van Tassel, P.R., Davis, H.T., and McCormick, A.V. New lattice model for adsorption of small molecules in zeolite micropores. *AIChE J.* 1994, **40,** 925–934

8 Van Tassel, P.R., Davis, H.T., and McCormick, A.V. Adsorption simulations of small molecules and their mixtures in a zeolite micropore. *Langmuir* 1994, **10,** 1257–1267

9 Keffer, D., McCormick, A.V., and Davis, H.T. Diffusion and percolation on zeolite sorption lattices. *J. Phys. Chem.* 1996, **100,** 967–973

10 Snurr, R.Q., Bell, A.T., and Theodorou, D.N. A hierarchical atomistic/lattice simulation approach for the prediction of adsorption thermodynamics of benzene in silicalite. *J. Phys. Chem.* 1994, **98,** 5111–5119

11 Nivarthi, S.S., Van Tassel, P.R., Davis, H.T., and McCormick, A.V. Adsorption and energetics of xenon in mordenite: A Monte Carlo simulation study. *J. Chem. Phys.* 1995, **103,** 3029–3037
12 Keffer, D., McCormick, A.V., and Davis, H.T. Unidirectional and single-file diffusion in $AlPO_4$-5: Molecular dynamics investigations. *Mol. Phys.* 1996, **87,** 367–387
13 Keffer, D., Davis, H.T., and McCormick, A.V. The effect of nanopore shape on the structure and isotherms of adsorbed fluids. *Adsorption* 1996, **2,** 9–21
14 Barri, S.A.I., Smith, G.W., White, D., and Young, D. Structure of Theta-1, the first unidimensional medium-pore high-silica zeolite. *Nature (London)* 1984, **312,** 533–534
15 Bennett, J.M., Cohen, J.P., Flanigen, E.M., Pluth, J.J., and Smith, J.V. Crystal structure of tetrapropylammonium hydroxide—aluminum phosphate number 5. *ACS Symp. Ser.* 1983, **218,** 109–118
16 Galli E. Mazzite, a zeolite. *Cryst. Struct. Commun.* 1974, **3,** 339–344
17 Newsam, J.M. Structural characterization of dehydrated gallium zeolite L. *Mater. Res. Bull.* 1986, **21,** 661–672
18 LaPierre, R.B., Rohrman, A.C., Jr., Schlenker, J.L., Wood, J.D., Rubin, M.K., and Rohrbaugh, W.J. The framework topology of ZSM-12: A high-silica zeolite. *Zeolites* 1985, **5,** 346–348
19 Dessau, R.M., Schlenker, J.L., and Higgins, J.B. Framework topology of $AlPO_4$-8: The first 14-ring molecular sieve. *Zeolites* 1990, **10,** 522–524
20 Richardson, J.W., Jr., Smith, J.V., and Pluth, J.J. Theoretical nets with 18-ring channels: Enumeration, geometrical modeling, and neutron diffraction study of $AlPO_4$-54. *J. Phys. Chem.* 1989, **93,** 8212–8219
21 Meier, W.M. The crystal structure of mordenite (ptilolite). *Z. Kristallogr.* 1961, **115,** 439–450
22 Olson, D.H., Kokotailo, G.T., Lawton, S.L., and Meier, W.M. Crystal structure and structure-related properties of ZSM-5. *J. Phys. Chem.* 1981, **85,** 2238–2243
23 Kokotailo, G.T., Chu, P., Lawton, S.L., and Meier, W.M. Synthesis and structure of synthetic zeolite ZSM-11. *Nature (London)* 1978, **275,** 119–120
24 Vaughan, P.A. The crystal structure of the zeolite ferrierite. *Acta Crystallogr.* 1966, **21,** 983–990
25 Newsam, J.M., Treacy, M.M.J., Koetsier, W.T., and de Gruyter, C.B. Structural characterization of zeolite beta. *Proc. R. Soc. Lond. A* 1988, **420,** 375–405
26 Gramlich, V., and Meier, W.M. The crystal structure of hydrated NaA: A detailed refinement of a pseudosymmetric zeolite structure. *Z. Kristallogr.* 1971, **133,** 134–149
27 Robson, H.E., Shoemaker, D.P., Oglivie, R.A., and Manor, P.C. Synthesis and crystal structure of zeolite Rho—a new zeolite related to Linde type A. *Adv. Chem. Ser.* 1973, **121,** 106–115
28 Fitch, A.N., Jobic, H., and Renoupres, A. Localization of benzene in sodium-Y zeolite by powder neutron diffraction. *J. Phys. Chem.* 1986, **90,** 1311–1318
29 Mortier, W.J., Pluth, J.J., and Smith, J.V. Positions of cations and molecules in zeolites with the chabazite framework. III. Dehydrated Na-exchanged chabazite. *Mater. Res. Bull.* 1977, **12,** 241–249
30 Estermann, M., McCusker, L.B., Baerlocher, C., Merrouche, A., and Kessler, H.A. synthetic gallophosphate molecular sieve with a 20-tetrahedral-atom pore opening. *Nature (London)* 1991, **352,** 320–323
31 Meier, W.M., Olson, D.H. *Atlas of Zeolite Structure Types,* 3rd Ed. Butterworth-Heinemann, London, 1992
32 Bezus, A.G., Kiselev, A.V., Lopatkin, A.A., and Pham Quang Du. Molecular statistical calculation of the thermodynamic adsorption characteristics of zeolites using the atom–atom approximation. Adsorption of methane by zeolite NaX. *J. Chem. Soc. Faraday Trans.* 1978, **74,** 367–379
33 Demontis, P., Fois, E.S., Suffriti, G.B., and Quartieri, S. Molecular dynamics studies on zeolites. 4. Diffusion of methane in silicalite. *J. Phys. Chem.* 1990, **94,** 4329–4334
34 Demontis, P., Suffritti, G.B., Fois, E.S., and Quartieri, S. Molecular dynamics studies on zeolites. 6. Temperature dependence of diffusion of methane in silicalite. *J. Phys. Chem.* 1992, **96,** 1482–1490
35 Nowak, A.K., Cheetham, A.K., Pickett, S.D., and Ramdas, S. A computer simulation of the adsorption and diffusion of benzene and toluene in the zeolites Theta-1 and silicate. *Mol. Simul.* 1987, **1,** 67–77
36 Vigne-Maeder, F., and Jobic, H. Adsorption sites and packing of benzene in silicalite. *Chem. Phys. Lett.* 1990, **169,** 31–35
37 Vigne-Maeder, F., and Auroux, A. Potential maps of methane, water, and methanol in silicalite. *J. Phys. Chem.* 1990, **94,** 316–322
38 June, R.L., Bell, A.T., and Theodorou, D.N. Molecular dynamics study of methane and xenon in silicalite. *J. Phys. Chem.* 1990, **94,** 8232–8240
39 June, R.L., Bell, A.T., and Theodorou, D.N. Transition-state studies of xenon and SF_6 diffusion in silicalite. *J. Phys. Chem.* 1991, **95,** 8866–8878
40 Goodbody, S.J., Watanabe, K., MacGowan, D., Walton, J.P.R.B., and Quirke, N. Molecular simulation of methane and butane in silicalite. *J. Chem. Soc. Faraday Trans.* 1991, **87,** 1951–1958
41 June, R.L., Bell, A.T., and Theodorou, D.N. Molecular dynamics studies of butane and hexane in silicalite. *J. Phys. Chem.* 1992, **96,** 1051–1060
42 Snurr, R.Q., Bell, A.T., and Theodorou, D.N. Prediction of adsorption of aromatic hydrocarbons in silicalite from grand canonical Monte Carlo simulations with biased insertions. *J. Phys. Chem.* 1993, **97,** 13472–13752
43 Nicholas, J.B., Trouw, F.R., Mertz, J.E., Iton, L.E., and Hopfinger, A.J. Molecular dynamics simulation of propane and methane in silicate. *J. Phys. Chem.* 1993, **97,** 4149–4163
44 Vigne-Maeder, F. Analysis of ^{129}Xe chemical shifts in zeolites from molecular dynamics calculations. *J. Phys. Chem.* 1994, **98,** 4666–4672
45 Smit, B., and Siepmann, J.I. Computer simulations of the energetics and siting of *n*-alkanes in zeolites. *J. Phys. Chem.* 1994, **98,** 8442–8452
46 Smit, B., and Maesen, T.L.M. Commensurate "freezing" of alkanes in the channels of a zeolite. *Nature (London)* 1995, **374,** 42–44

47 Vernov, A.V., and Steele, W.A. Sorption of xenon in zeolite Rho: A Thermodynamics/simulation study. *J. Phys. Chem.* 1993, **97,** 7660–7664
48 Loriso, A., Bojan, M.J., Vernov, A., and Steele, W.A. Computer simulation studies of ordered structures formed by rare gases sorbed in zeolite Rho. *J. Phys. Chem.* 1993, **97,** 7665–7671
49 Soto, J.L., and Myers, A.L. Monte Carlo studies of adsorption in molecular sieves. *Mol. Phys.* 1981, **42,** 971–983
50 Yashonath, S., Thomas, J.M., Novak, A.K., and Cheetham, A.K. The siting, energetics and mobility of saturated hydrocarbons inside zeolitic cages: Methane in zeolite Y. *Nature (London)* 1988, **331,** 601–604
51 Yashonath, S., Demontis, P., and Klein, M.L. A molecular dynamics study of methane in zeolite NaY. *Chem. Phys. Lett.* 1988, **153,** 551–556
52 Woods, G.B., Panagiotopoulos, A.Z., and Rowlinson, J.S. Adsorption of fluids in model zeolite cavities. *Mol. Phys.* 1988, **63,** 49–63
53 Woods, G.B. and Rowlinson, J.S. Computer simulations of fluids in zeolites X and Y. *J. Chem. Soc. Faraday Trans.* 1989, **85,** 765–781
54 Demontis, P., Yashonath, S., and Klein, M.L. Location and mobility of benzene in sodium-Y zeolite by molecular dynamics calculations. *J. Phys. Chem.* 1989, **93,** 5016–5019
55 Yashonath, S. A molecular dynamics study of cage-to-cage migration in sodium Y zeolite: Role of surface-mediated diffusion. *J. Phys. Chem.* 1991, **95,** 5877–5881
56 Yashonath, S., Demontis, P., and Klein, M.L. Temperature and concentration dependence of adsorption properties of methane in NaY: A molecular dynamics study. *J. Phys. Chem.* 1991, **95,** 5881–5889
57 Santikary, P., Yashonath, S., and Ananthakrishna, G. A molecular dynamics study of xenon sorbed in sodium Y zeolite. 1. Temperature and concentration dependence. *J. Phys. Chem.* 1992, **96,** 10469–10477
58 Yashonath, S., and Santikary, P. Xenon in sodium Y zeolite. 2. Arrhenius relation, mechanism, and barrier height distribution for cage-to-cage diffusion. *J. Phys. Chem.* 1993, **97,** 3849–3857
59 Yashonath, S., and Santikary, P. Diffusion of sorbates in zeolites Y and A: Novel dependence of sorbate size and strength of sorbate-zeolite interaction. *J. Phys. Chem.* 1994, **98,** 6368–6376
60 Klein, H., Kirschhock, C., and Fuess, H. Adsorption and diffusion of aromatic hydrocarbons in zeolite Y by molecular mechanics calculation and x-ray powder diffraction. *J. Phys. Chem.* 1994, **98,** 12345–12360
61 Gupta, V., Davis, H.T., and McCormick, A.V. Comparison of ^{129}Xe chemical shift simulation in siliceous zeolite Y. *J. Phys. Chem.*, in press, 1996
62 Keffer, D. Ph.D. thesis. University of Minnesota, Minneapolis, Minnesota, 1996